

RESEARCH ARTICLE OPEN ACCESS

A Global Analysis of Historical and Future Changes in Mediterranean Climate-Type Regions

Diego Urdiales-Flores^{1,2}  | George Zittis²  | Panos Hadjinicolaou²  | Annalisa Cherchi^{3,4}  | Andrea Alessandri³  | Nadav Peleg^{1,5}  | Jos Lelieveld^{2,6} 

¹Institute of Earth Surface Dynamics, University of Lausanne, Lausanne, Switzerland | ²Climate and Atmosphere Research Center (CARE-C), The Cyprus Institute, Nicosia, Cyprus | ³National Research Council, Institute of the Atmospheric Sciences and Climate (CNR-ISAC), Bologna, Italy | ⁴Istituto Nazionale di Geofisica e Vulcanologia (INGV), Bologna, Italy | ⁵Expertise Center for Climate Extremes, University of Lausanne, Lausanne, Switzerland | ⁶Atmospheric Chemistry Department, Max Planck Institute for Chemistry, Mainz, Germany

Correspondence: Diego Urdiales-Flores (diego.urdialesflores@unil.ch; d.flores@cyi.ac.cy)

Received: 12 September 2023 | **Revised:** 20 May 2024 | **Accepted:** 6 October 2024

Funding: This work was supported by the EMME-CARE project that has received funding from the European Union's Horizon 2020 Research and Innovation Program, under Grant Agreement No. 856612, as well as matching co-funding by the Government of Cyprus. D.U.F. was supported by the Swiss Government Excellence Scholarship 2023/2024 that has received funding from Swiss State Secretariat for Education and Innovation. G.Z., A.C. and A.A. were funded by the European Union's Horizon Europe Research and Innovation Program under Grant Agreement No. 101081193 (OptimESM project). A.C. and A.A. acknowledge support from ICSC—Centro Nazionale di Ricerca in High Performance Computing, Big Data and Quantum Computing, funded by European Union—NextGenerationEU (Concession Decree N. 1031 of 17/06/2022 adopted by the Italian Ministry of University and Research). N.P. was supported by the Swiss National Science Foundation (SNSF), Grant 194649 ('Rainfall and floods in future cities').

Keywords: climate change | Mediterranean-type climates | projection and prediction

ABSTRACT

Mediterranean climate-type regions (MCRs) are characterised by warm-to-hot dry summers and mild-wet winters. These regions are typically found on the western or southern edges of continents, for example, in the Mediterranean Basin, the west coast of North and South America, southern Africa and southwest Australia. The MCRs are vulnerable to climate variability and change related to their unique characteristics, such as pronounced rainfall seasonality and prolonged hot and dry summers. Based on historical observations and CMIP6 climate projections, we apply an empirical bio-climatic assessment of how the geographic distribution of MCRs has changed during the last century and how these zones will be further impacted under continued warming. Results indicate a poleward and eastward expansion of MCRs in the Mediterranean Basin, North America-California and South America-Central Chile regions. For parts of Southern Africa and Southern Australia, a retreat of the MCR margins and an expansion of more arid climate zones are projected. These shifts are particularly profound according to high emission and radiative forcing pathways and future scenarios. The warming in MCRs is projected to accelerate (e.g., mean regional warming of up to 5.5°C under a 4°C global warming scenario), and precipitation will decrease by about 5%–10% for every additional degree of global warming. One exception is the California MCR, where rainfall will likely increase. Such changes can challenge water resources, food security and other aspects of human livelihood and ecosystems in these unique geographical zones.

1 | Introduction

Mediterranean climate-type regions (MCRs) are mid-latitude transitional climate zones broadly characterised by wet winters and dry summers (Alessandri et al. 2014; Seager

et al. 2019). MCRs are typically found on the western sides of the world's continents, wedged between temperate (mostly poleward), cold-winter (eastward and poleward) and arid (equatorward) climates (Beck et al. 2018; Kottek et al. 2006). These regions are primarily affected by storm tracks in

This is an open access article under the terms of the [Creative Commons Attribution](https://creativecommons.org/licenses/by/4.0/) License, which permits use, distribution and reproduction in any medium, provided the original work is properly cited.

© 2024 The Authors. *International Journal of Climatology* published by John Wiley & Sons Ltd on behalf of Royal Meteorological Society.

winter and subtropical anticyclones in summer (Alessandri et al. 2014; Cherchi et al. 2018; Deitch, Sapundjieff, and Feirer 2017; Rodwell and Hoskins 2001; Seager et al. 2003). Water resources in MCRs are volatile from year-to-year or season-to-season due to the high spatiotemporal variability of rainfall. For example, one large storm can make an inordinate difference to the total annual precipitation budget (Campins et al. 2011; Flocas et al. 2010; Zittis, Bruggeman, and Lelieveld 2021). Summers are typically dry, apart from localised convection over elevated land, while the subtropical location and clear skies under descending air lead to high temperatures (Seager et al. 2019).

There are five main locations in the world with such characteristics. These are parts of the Mediterranean Basin (MED), the west coast of North America-California, from Northern Mexico to Washington State (NAC), South America-Central Chile (SAC), Southern Africa (SAF) and Southern Australia (SAU) (Figure 1). These regions currently correspond to approximately 2% of the Earth's land surface but are home to more than 700 million people, or nearly 10% of the global population (Urdiales-Flores et al. 2023). Due to their temperate environmental characteristics, they are biodiversity hotspots as well as one of the most desired climatic zones for human inhabitation and tourism (Myers et al. 2000; Vogiatzakis, Mannion, and Sarris 2016). Owing to the high levels of endemism, numerous high conservation priority hotspots are located in the temperate zones of the Mediterranean Basin, the California Floristic Province, Central Chile, the Cape Floristic Province and Southwest Australia (Myers et al. 2000). For example, cultivars of significant economic and cultural value, such as viticulture, are concentrated in Mediterranean climate-type regions due to their distinctive climate characteristics, while they are susceptible to changes in environmental conditions (Hannah et al. 2013).

During the past century, MCRs have warmed similarly to the global mean, except for the Mediterranean Basin, which has experienced accelerated warming (nearly two times faster than the global mean rates), mainly during the last four decades (Urdiales-Flores et al. 2023; Zittis et al. 2022). The observed precipitation trends point to overall drying in many MCRs, but these changes are associated with many uncertainties (Morin 2011), and their drivers are not fully understood. The lack of systematic

and spatiotemporally consistent observations in some MCRs (e.g., parts of North Africa, central Chile, Southern Africa) and inconsistencies in the techniques used for data blending and gridding can partially over parts of Southern Australia and North America-California account for these uncertainties (Sylla et al. 2013; Behnke et al. 2016; Lazenby et al. 2018; Urdiales et al. 2018; Zittis 2018; Chua et al. 2022; Dey et al. 2019; Araya-Osses et al. 2020). Some studies identified an important role for anthropogenic forcing, including increasing greenhouse gas emissions (Cheng et al. 2022), stratospheric ozone depletion (Kang et al. 2011; Min and Son 2013), and changes in anthropogenic aerosols (Allen and Ajoku 2016; Kovilakam and Mahajan 2015). While, other studies concluded that the observed precipitation changes are within the range of natural climate variability (Amaya et al. 2018; Mantsis et al. 2017). In any case, future changes in the hydrological cycle, can be robust and significant, at least for certain regions, scenarios, or future periods, and are expected to occur under a warmer climate (Lionello and Scarascia 2018; Zittis et al. 2019; Cherif et al. 2020; Douville et al. 2021).

Given the similarity of the MCRs' main climate and environmental characteristics, their comparable geographic locations and planetary-scale atmospheric circulation influences, the causes and nature of climate variability and change are expected to be similar in all Mediterranean climate-type regions. Due to their subtropical to midlatitude setting, variability is expected to be mainly influenced by the tropics and via annular variability modes. Nevertheless, tropically forced variability primarily arises from the Pacific, and hence, it is not surprising that the North American West Coast and Chile are primarily affected (Cai et al. 2015). Although the El Niño-Southern Oscillation (ENSO) induced variability is global, the other MCRs are in locations remote from the tropical Pacific and/or near nodal lines in ENSO-teleconnections (Taschetto et al. 2020). Therefore, other natural variability modes, like the North Atlantic Oscillation (NAO), have a greater influence (Mariotti and Dell'Aquila 2012; Barcikowska et al. 2020).

Extensive literature on climate variability and change in MED, NAC, and, to some extent, SAC has become available recently. The number of regional studies is somewhat less for SAF and SAU. For example, Urdiales-Flores et al. (2023) identified the

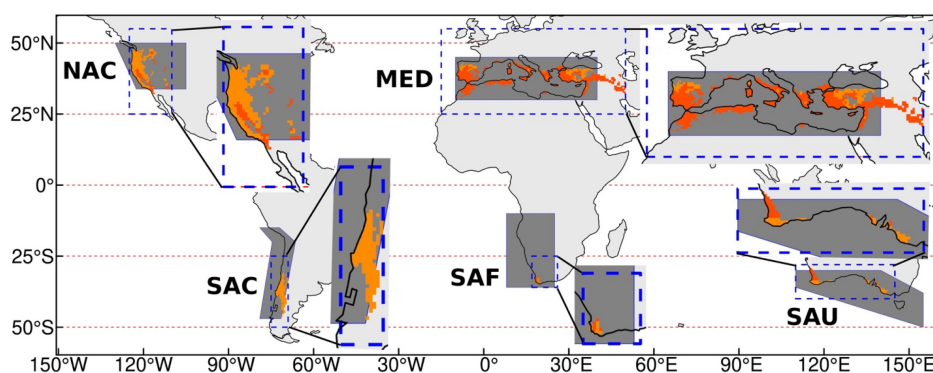


FIGURE 1 | The Mediterranean climate-type regions (dry summer climate zones with hot summers—Csa in red, and warm summer conditions—Csb in orange) for 1991–2020 (based on CRU-TS v4.05 dataset). The IPCC Working Group I regions with Mediterranean climate types are grey-shaded for reference. Blue dashed boxes represent the regional domains used in this study (MED: Mediterranean Basin; NAC: North America-California; SAC: South America-Central Chile; SAF: Southern Africa; SAU: Southern Australia) and are zoomed to better distinguish Csa and Csb colours.

dominant drivers of temperature variability in global MCRs during the last four decades (i.e., greenhouse gas forcing, trends in aerosols, and land-atmosphere interactions) and quantified their contribution to the observed warming. Seager et al. (2019) and Deitch, Sapundjieff, and Feirer (2017) addressed the mechanistic climate dynamics framework of temperature and precipitation, while Polade et al. (2017) and Alessandri et al. (2014) assessed their potential expansion or retreat under future conditions. Compared to other MCRs, the MED has been more intensively studied, and large initiatives have provided comprehensive climate change assessments for the past and the future (Lionello 2012; Cherif et al. 2020; Fatichi et al. 2021; Ali et al. 2022).

Considering the importance and sensitivity of these marginal climate regimes, the present study aims to explore the historical and possible future evolution of Mediterranean climate-type regions on a global scale. Using the widely-used Köppen-Geiger climate classification and an ensemble of statistically-downscaled and bias-corrected climate projections, appropriate for such analyses, our main objective is to understand changes and potential shifts to different temperature and precipitation regimes. To be compliant with discussions on climate change mitigation, we focus on critical future global warming levels from 1.5°C to 4°C relative to the pre-industrial era.

This approach is novel compared to previous studies (Polade et al. 2017; Alessandri et al. 2014), and together with the use of updated observations, refined climate projections and scenarios, using bias-adjusted data, it provides a revised and more comprehensive analysis, thus contributing to a better understanding of how climate change can impact mid-latitude regions such as Mediterranean-type environments.

2 | Data and Methods

2.1 | Köppen-Geiger Climate Classification

We applied the Köppen-Geiger climate classification, conceived by Köppen (1900) and updated more recently (Beck et al. 2018; Kottek et al. 2006). It is an empirical bio-climatic classification aimed at defining climatic attributes in correspondence with those of specific vegetation zones. In Table S1, we summarise the main characteristics of the Arid (B), warm Temperate (C), and Snow (D) climate types that are most common in mid-latitude regions. The Mediterranean climate type is defined here as the warm temperate, dry summer zones with hot (Csa) and warm summer conditions (Csb). For example, in these zones, the mean temperature of the coldest month ranges from -3°C to 18°C . Precipitation is substantially higher during winter, while it is below 40 mm in the driest month of the year.

In both hemispheres, the progression to wetter and drier conditions marks the transition to other warm-temperate climates poleward and arid climates equatorward, respectively. Conversely, the much colder conditions, mainly during the winter months, characterise the transition to the snow climate zones that are found in higher latitudes or higher-elevation areas and mountains (Table S1). MCRs were determined by including all land grid cells meeting the criteria of Table S1, within the

following five domains (Figure 1): (i) the Mediterranean Basin (15°W to 50°E , 25°N to 55°N); (ii) North America-California (125°W to 110°W , 25°N to 55°N); (iii) South America-Central Chile (75°W to 69°E , 50°S to 25°S); (iv) Southern Africa (26°E to 17°E , 36°S to 25°S); and (v) Southern Australia (145°E to 110°E , 40°N to 28°N).

2.2 | Climate Data

We use historical simulations (1850–2014) and future climate projections (2015–2100) from five Global Earth System Models (ESMs), available from the World Climate Research Program Coupled Model Intercomparison Project Phase 6 (CMIP6) (Petrie et al. 2021; Tebaldi et al. 2021). These five models' results are publicly available as bias-corrected and statistically-downscaled to a standard spatial grid of $0.5^{\circ}\times 0.5^{\circ}$ resolution (Lange and Büchner 2021). In particular, these ESMs' outputs are corrected based on a statistical bias correction algorithm used in the Water Model Intercomparison Project (WaterMIP) and Water and Global Change (WATCH) initiatives to correct temperature values (Hagemann et al. 2011; Piani et al. 2010). Monthly correction factors are derived over a construction period of 40 years, where the ESM output is compared to the observation-based WATCH forcing data. The ESM data are also interpolated to the spatial resolution of the WATCH data set ($0.5^{\circ}\times 0.5^{\circ}$). For each month, a regression is performed on the ranked data sets. Subsequently, the derived monthly correction factors are interpolated towards daily ones. The same correction factors are then applied to projected ESM data. This method is skillful in conserving robustness properties and eliminating unrealistic jumps at seasonal or monthly transitions (Piani et al. 2010). Since monthly values are used for the Köppen-Geiger climate classification, the treatment of extremes is not expected to influence our analysis significantly and was therefore not assessed. More details in this processing are available in the Intersectoral Impact Model Intercomparison Project (ISI-MIP) protocol.¹

The historical simulations are based on observed concentrations of atmospheric constituents and other forcings, including greenhouse gases (GHGs), anthropogenic aerosols, ozone, solar irradiance, and land-use change (IPCC 2021). The projections are forced with a future scenario of the same drivers, defined by Shared Socio-economic Pathways—SSPs (Petrie et al. 2021). As we intend to focus the analysis in terms of GWLs, among the various pathway families, we selected the most extreme one (SSP5-8.5), which implies higher radiative forcing and that can provide a broader range of potential warming levels. The radiative forcing under SSP5-8.5 is projected to increase throughout the 21st century, reaching 8.5 W m^{-2} by 2100. The ESMs used in this study are GFDL-ESM4, IPSL-CM6A-LR, MPI-ESM1-2-HR, MRI-ESM2-0 and UKESM1-0-LL (see Table S2). The dataset is limited to one model realisation, or ensemble member, for each ESM. This selection is based on the availability of bias-adjusted and statistically-downscaled fields, which are required for such applications. Since the climate classification is based on critical thresholds of temperature and precipitation, systematic biases could substantially impact the representation of climate zones. Noteworthy, this ensemble provides a representative range of model-effective climate sensitivities and, thus, possible future projections (Zelinka et al. 2020).

To compare the selected CMIP6 historical simulations we use two gridded observational datasets: the CRU-TS Version 4.05 (Harris et al. 2020) and ISI-MIP3a Version 1.0 (Lange and Büchner 2020). Both datasets are monthly mean near-surface (2m) temperature (tmp), maximum temperature (tmx), minimum temperature (tmn), and precipitation (pre). This comparison is performed in the form of global maps for the last 30 years of the historical simulations (1985–2014) and a comparison of the area (in km²) described as MCR for every 30 years from 1901 to 2020. All data were remapped and analysed in a standard resolution (0.5° × 0.5°), matching the spatial grid structure of the downscaled CMIP6 models selected.

2.3 | Definition of Global Warming Levels

For future projections, instead of the standard approach of presenting results as time-slice averages (e.g., mid-century, end-century, etc.), we performed the analysis on several global warming levels (GWLs). This provides a comprehensible view of future climate evolutions in the context of policymaking and climate mitigation targets. It also allows intercomparison with previous studies based on different sets of scenarios of model ensembles. Based on the CMIP6 projections, we define the points in time for which the 1.5°C, 2°C, 3°C and 4°C transient GWLs are exceeded relative to the 1850–1900 approximation of the pre-industrial era. These points in time were calculated as the central year of the 20-year moving window where any of the selected GWLs is first reached. The 20-year moving window method is here chosen to be consistent with the methodologies applied in the IPCC Working Group I Atlas of Regional Information² and is similar to what is described in other studies (e.g., Liu et al. 2021; Nikulin et al. 2018). The centre years for reaching the selected GWLs are presented in Table S2. For the future projections, we estimated the extent of MCRs by applying the Köppen-Geiger climate classification based on the ensemble mean values of monthly temperature and precipitation after being averaged for the 20-year periods used in the definition of GWLs.

2.4 | Regional Temperature and Precipitation Projections

In addition to the GWLs analysis, we explore temperature and precipitation projections relative to the reference pre-industrial (1850–1900) and recent past (1985–2014) periods, respectively. The latter includes the last 30 years of historical CMIP6 simulations. The regional domains defined in Sub-section 2.1 and presented in Figure 1 were used for calculating the regional changes. Land-only, area-weighted averages were used to provide a summary of the results for each MCR and for every GWL.

3 | Results

3.1 | Comparison With Observations

The global maps of the Köppen-Geiger climate classification based on the CRU gridded observations and the historical CMIP6 simulations (using the multi-model ensemble mean) are presented in Figure 2. Overall, the spatial extent of the model-derived

classification fits well with the observations for the 1985–2014 reference period. The one-to-one grid cell absolute agreement in the spatial distribution of climate zones, including all sub-classifications, is about 95%. This apparent agreement between the simulated and observed conditions is expected since the CMIP6 data used in the present study are bias-adjusted and statistically downscaled to a spatial resolution close to the gridded observations. Although there is a general consensus, there are some disparities between the classification results obtained through the CRU observations and those generated by the CMIP6 models (historical runs). These differences are highlighted in red in Figure 2; none of them are overlapping with the Mediterranean climate-type regions. For example, CRU classifies Antarctica as ET (Polar Tundra climate), whereas in the CMIP6 models, it is represented as EF (Polar Ice Cap climate). Less profound differences can be found in other areas, such as parts of Central USA, tropical South America or limited regions in the Tibetan Plateau. The representation of Mediterranean climate-type zones (Csa and Csb) agrees between the two datasets (see Table S3).

Table S3 provides a detailed comparison of the simulated (CMIP6-based) and observed (CRU-based) percentages of global land area for all climate classes during the period 1985–2014. Globally, the dominant climate class by land area is Arid—B (CRU: 31.9%, CMIP6: 31.8%), followed by Cold—D (CRU: 22.5%, CMIP6: 23%), Tropical—A (CRU: 18.5%, CMIP6: 19%), Temperate—C (CRU: 15%, CMIP6: 13.5%), and Polar—E (CRU: 12%, CMIP6: 12.7%). The most common individual climate type by land area is hot desert—BWh (CRU: 14%, CMIP6: 14.2%), followed by tropical dry-winter Savanna—Aw (CRU: 11.4%, CMIP6: 11.5%).

The Mediterranean climate types, considered as the Csa and Csb subcategories, cover nearly 2.4% of the global land area and are primarily located at the mid-latitude zones of each hemisphere (mostly between 25° and 50° north and south), at the western edges of continents over the coasts (Figures 1 and 2). The CMIP6 models slightly underestimate their total area by 0.4% (Table S3). For a more detailed visual comparison of the Köppen-Geiger classification between the observed and simulated conditions, the maps of Figure 2 are also presented at a higher resolution, with zooms on each MCR (Figures S1–S5).

An additional comparison of the extent estimation of Csa and Csb in terms of land area is presented every 30 years during the last 120 years (i.e., 1901–1930, 1931–1960, 1961–1990, 1991–2020). Both CRU and ISI-MIP are displayed here as a reference to account for the uncertainty in the observations. The comparison with CMIP6 is provided in the left part of Figure 3 (orange-shaded), bottom panels of Figures 4 and 5 and Figures S6–S8. The mean and maximum bias of Csa and Csb zones between observed (CRU and ISI-MIP) and historical simulated (CMIP6) during the period 1901–2020 range between 4×10^4 km² and 25.4×10^4 km² or –1.3% and –8.1% of their total area, respectively. The area underestimation by the CMIP6 models is more evident in the early 20th century (1901–1930) and for the Csb class (warm summer temperate zone).

3.2 | Spatiotemporal Evolution of Global MCRs

Considering the historical evolution during the last 120 years, the extent of global MCRs (Csa + Csb) has not changed much

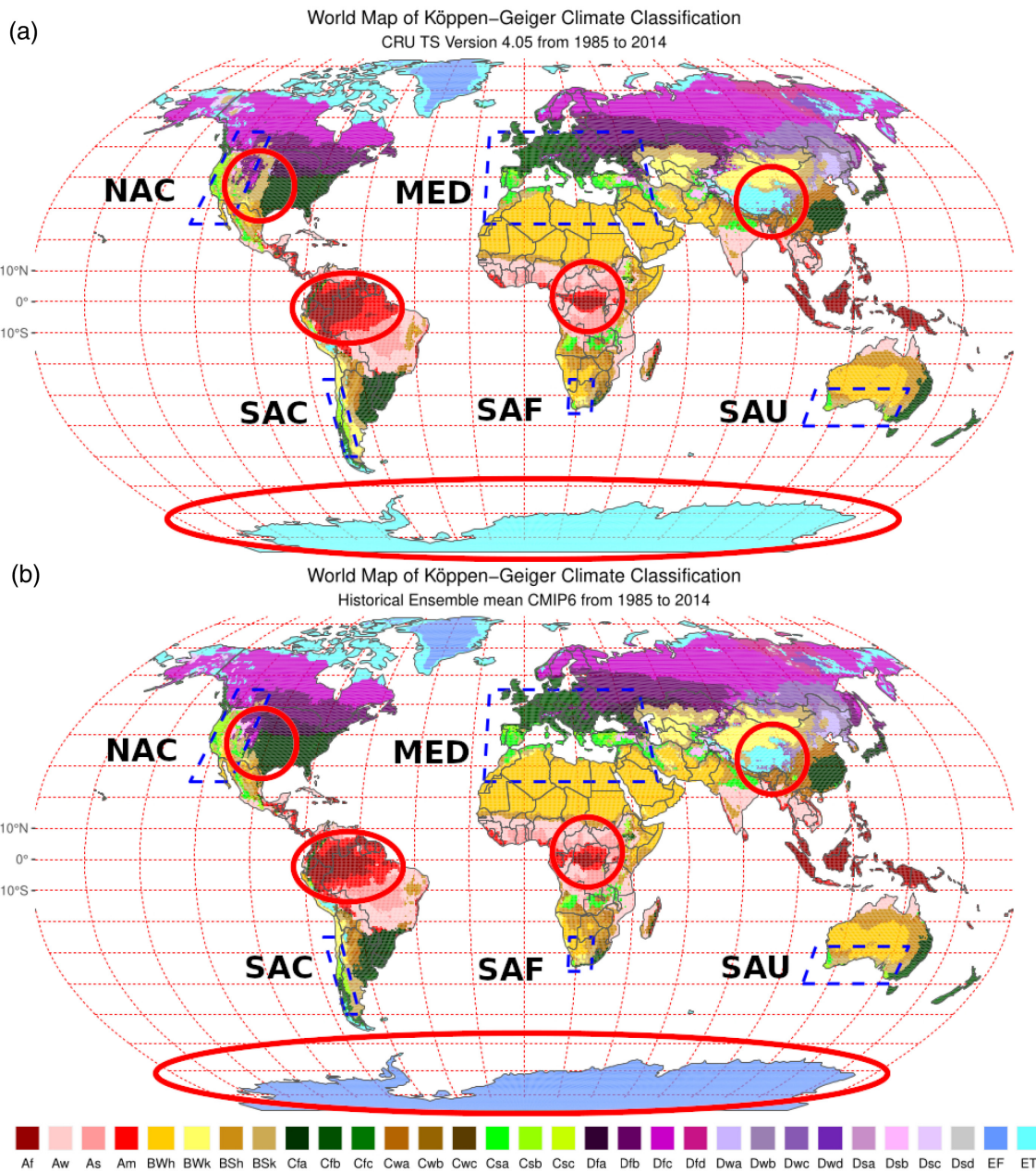


FIGURE 2 | Global maps of the Köppen-Geiger climate classification (1985–2014), based on (a) the CRU gridded observations (v4.05) and (b) the historical CMIP6 simulations (ensemble mean). Blue dashed boxes represent the domains used to calculate Mediterranean climate-type regions. Regions with profound differences are enclosed in the red circles.

regarding their total area. For example, during the period 1901–2020, the average total area is around $292 \times 10^4 \text{ km}^2$ and $288 \times 10^4 \text{ km}^2$ considering observed (CRU and ISI-MIP) and simulated historical conditions (CMIP6), respectively (Figure 3). The breakdown into subcategories reveals that Csb regions have decreased by 8.1%. In comparison, Csa areas increased by 9.5%, probably driven by the intense warming observed in these regions (e.g., Urdales-Flores et al. 2023) rather than changes in the hydrological cycle.

For the future, the total projected area is similar for all investigated GWLs ($\sim 305 \times 10^4 \text{ km}^2$). Global MCRs extent will likely expand by about 5.8% or $18 \times 10^4 \text{ km}^2$. This is mostly due to the

substantial areal expansion of global Csa zones (hot-summer class). With increasing temperatures, these are projected to expand by up to 52%, with respect to the recent past (1991–2020), exceeding $270 \times 10^4 \text{ km}^2$ at the 4°C GWL (Figure 3). This expansion will be at the expense of the warm-summer class (Csb), which in a warmer world is projected to decrease significantly. This retreat will likely reach 70% of its recent-past extent or $32.3 \times 10^4 \text{ km}^2$ at the highest global warming levels. In a worldwide context, MCRs' total area is projected to decrease slightly (0.33% decrease in global land area). This is mainly associated with the retreat of warm-summer temperate zones (Csb), which are projected to drastically decrease in extent by up to 0.36% (Table S4).

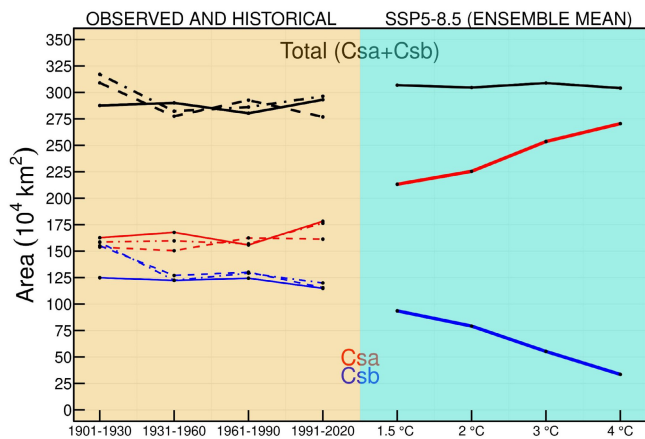


FIGURE 3 | Land area (in km²) as a function of time (historical: Orange-shaded) and future global warming levels (cyan-shaded) for Csa (red), Csb (blue) categories of the Köppen-Geiger classification and their total extend (black). The solid lines represent the CMIP6 multi-model ensemble, dashed lines the CRU and dashed-dotted the ISI-MIP observations. The historical CMIP6 simulations are based on the period 1901–2014, plus 6 years from the scenario runs 2015–2020.

To investigate the expansion and retreat of zones under historical and future conditions in more detail, we calculated the area (percentage of total land area) for three main categories (Arid—B, Temperate—C, excl. Csa and Csb, Snow—D) and two subcategories (hot-summer—Csa and warm summer—Csb), for the historical period (1901–2020) and future GWLs (Table 1). These calculations were applied to the regional domains defined in Sub-section 2.1. For the historical 120-year period, the Arid (B) zone expansion is evident in all regions except NAC. In MED, SAC, SAF and SAU, this is estimated to be +1.4%, +9.7%, +0.2% and +2.2%, respectively, in terms of the total area of regional domains specified in Figure 1 (see also Table 1). This expansion is mainly at the expense of Temperate (C) or Cold (D) zones. The latter is particularly evident in the MED and NAC regions, where the retreat of snow regimes is almost 5% in terms of land area. The overall retreat of MCRs zones is more robust in SAF and SAU regions (2.1% and 2.4%, respectively).

A comparison between the most recent historical period (1991–2020) and future projections (GWLs) reveals an expansion of arid regimes (class B) in most MCRs (see Table 1). In MED, NAC, SAC, SAF and SAU, a retreat of the Csb subcategory is projected to be up to –2%, –12.4%, –25.2%, 2.6% and 3.2%, of their recent past extent, respectively. The most robust retreat is expected for the highest GWLs. The hot-summer temperate zones (Csa) will likely expand by 0.8% in MED, 15.5% in NAC, 6.4% in SAC, 1.8% in SAF and 0.9% in SAU. The snow zones (class D) that were more widespread in the MED and NAC regional domains are projected to retreat, particularly at high warming levels and in the MED region. Under such scenarios, these zones will likely cover less than 5% of the area, as defined in Sub-section 2.1.

3.3 | Geographical Shifts of MCRs

The expansion or retreat of MCR zones in some regions occurs at the expense of adjacent climatic zones and vice versa. Here, we highlight three types of changes (i.e., colour shading

in Figure 4a,b and Figure 5a,b) indicating ‘total’, ‘partial’ and ‘minor’ in each land grid. These classifications are determined for each grid point based on the transition observed across four (total), three (partial) and two (minor) temporal cutoffs, considering 4 tranches of historical simulations (i.e., 1901–1930, 1931–1960, 1961–1990, 1991–2020; Figures 4a and 5a) or GWL thresholds in future projections (i.e., 1.5°C, 2°C, 3°C and 4°C transient GWLs; Figures 4b and 5b).

In terms of historical changes, the MED region has undergone a ‘total’ change in limited parts of southern Europe (mainly in the Iberian Peninsula) and, to a lesser extent, in northern Africa (see Figure 4a). The future estimates for MED, considering potential changes of all GWLs, suggest robust changes with a poleward and eastward expansion of MCRs being evident (Figure 4b,c). The corresponding MED area expansion in the latitude band between 37° N and 55° N experiences the most profound area increase at around 47° N, with emerging MCRs in parts of France, and southern and eastern Europe (Figure 4c). In addition, there is a reduction of the temperate zone area coverage on the equatorward flank, as shown by the area in the band at latitudes lower than 36° N, which are more prominent in the historical simulations compared to the future projections.

In North America, Oregon, Idaho, Nevada, Utah, and Arizona are the states where there have been ‘partial’ or ‘total’ changes during the historical period (Figure 5a). In contrast, the CMIP6 models project ‘partial’ and ‘total’ changes in several areas in southern Arizona and Mexico, where MCRs were not present during the last 120 years. The expansion in the area is projected to peak at 43° N (Figure 5c), but expansions to latitudes well above 50° N are also highlighted. Like the MED region, the NAC southern margins in southern California, southern Arizona and northern Mexico will likely be replaced by more arid zones (see also Table 1). The future transition from Csb to Csa zones is profound. Particularly at GWLs higher than 1.5°C, Csa zones are becoming dominant in the region (Figure 5d).

In SAC, most historical changes are found in the Concepcion and Temuco regions (Figure S6). For the future, a robust eastward expansion of the MCR zones is projected, while a transition from Csb to Csa zones is also evident, mainly for the highest GWLs. For SAF, the change of categories has affected all the areas surrounding Cape Town, with the historical and future retreat of Csb zones being more robust than the increase of the Csa (Figure S7). Finally, SAU has faced a substantial change of regimes in Melbourne, Adelaide and Eastern Perth, while future projections indicate a westward retreat of the MCR zones (Figure S8).

3.4 | Regional Temperature and Precipitation Responses to Global Warming

The regional warming will likely continue to be more pronounced than the global average, particularly in the Northern Hemisphere MCRs (Figure 6). On average, the regional temperature will likely increase by more than 1°C in the Mediterranean Basin and North America-California for every

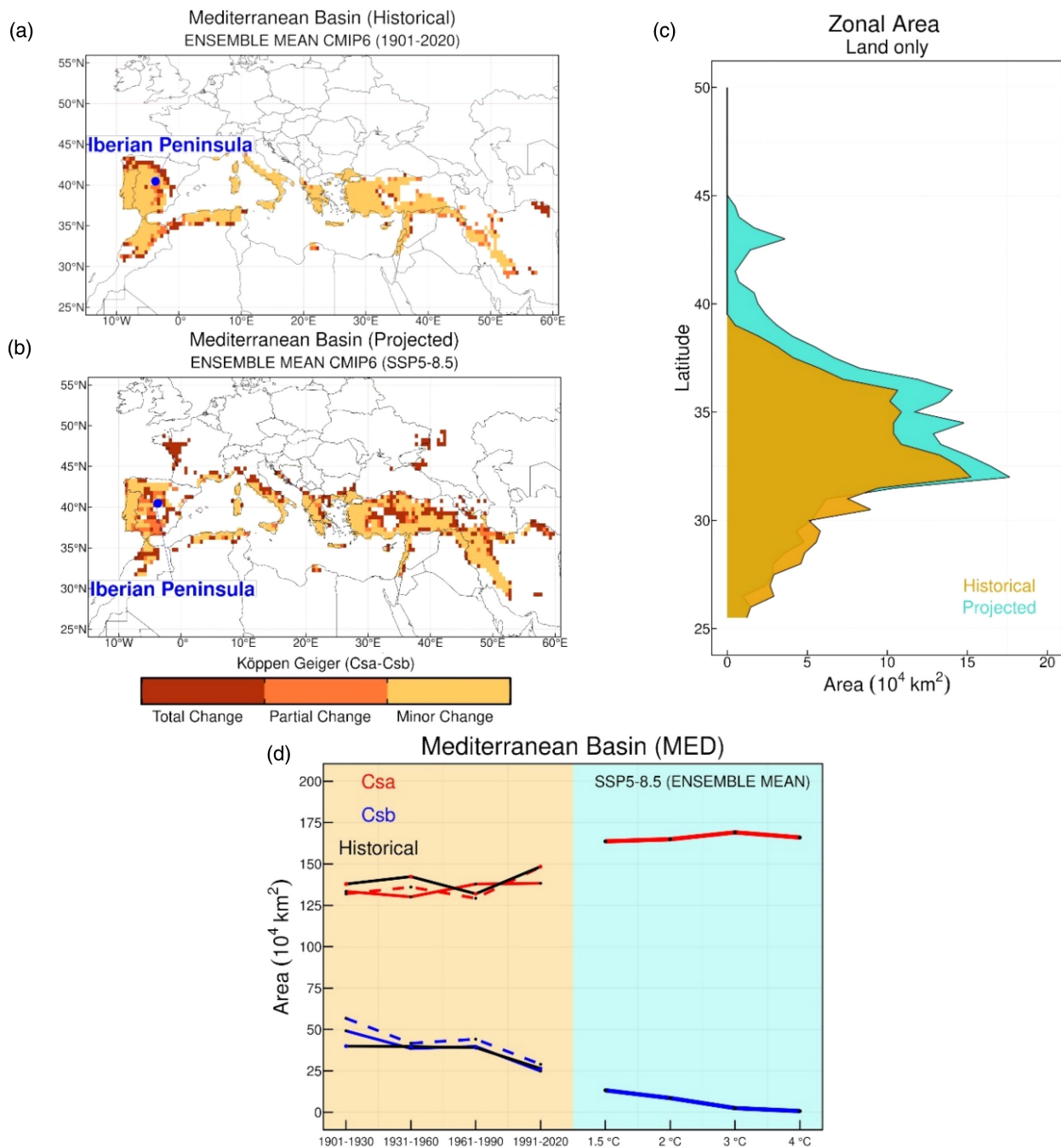


FIGURE 4 | Historical (a) and future (b) spatial distribution of Mediterranean climate-type zones in the Mediterranean Basin. See the text for the description of ‘total’, ‘partial’ and ‘minor’ changes. Zonal area considering historical simulations and projected changes (c). The colours in panel c are two (gold for historical and cyan for projections), but when they overlap the nuance changes. Temporal evolution of Csa and Csb climate zones (d). In panel (d), solid lines represent the CMIP6 multi-model ensemble, and dashed lines are the CRU and dashed-dotted ISI-MIP observations.

degree of GWL. The warming is expected to be up to 5.5°C (with respect to pre-industrial conditions) at 4°C GWL or even reach 6°C for the models with the higher climate sensitivity. Note that both the global and regional temperature changes refer to land-only areas. On the other hand, in South America-Central Chile (SAC), Southern Africa (SAF) and Southern Australia (SAU), the future regional warming will be less pronounced yet still more robust than the global average. For example, for a 4°C GWL, the regional anomalies will be between 4.3°C and 5.3°C.

Figure 7 illustrates the regional precipitation changes for different GWLs since the pre-industrial era. Although for all GWLs (1.5°C to 4°C) over Northern Hemisphere MCRs, the CMIP6 projections agree overall regarding the sign and magnitude of changes, this is not the case for MCRs in the Southern Hemisphere. Such inconsistencies are more evident in South America-Central Chile (SAC) and Southern Africa (SAF). For example, the MPI-ESM1-2-HR model over SAC projected a substantial precipitation decrease between 35% and 50%, while the multi-model ensemble for the highest GWL (4°C) suggests more moderate declines

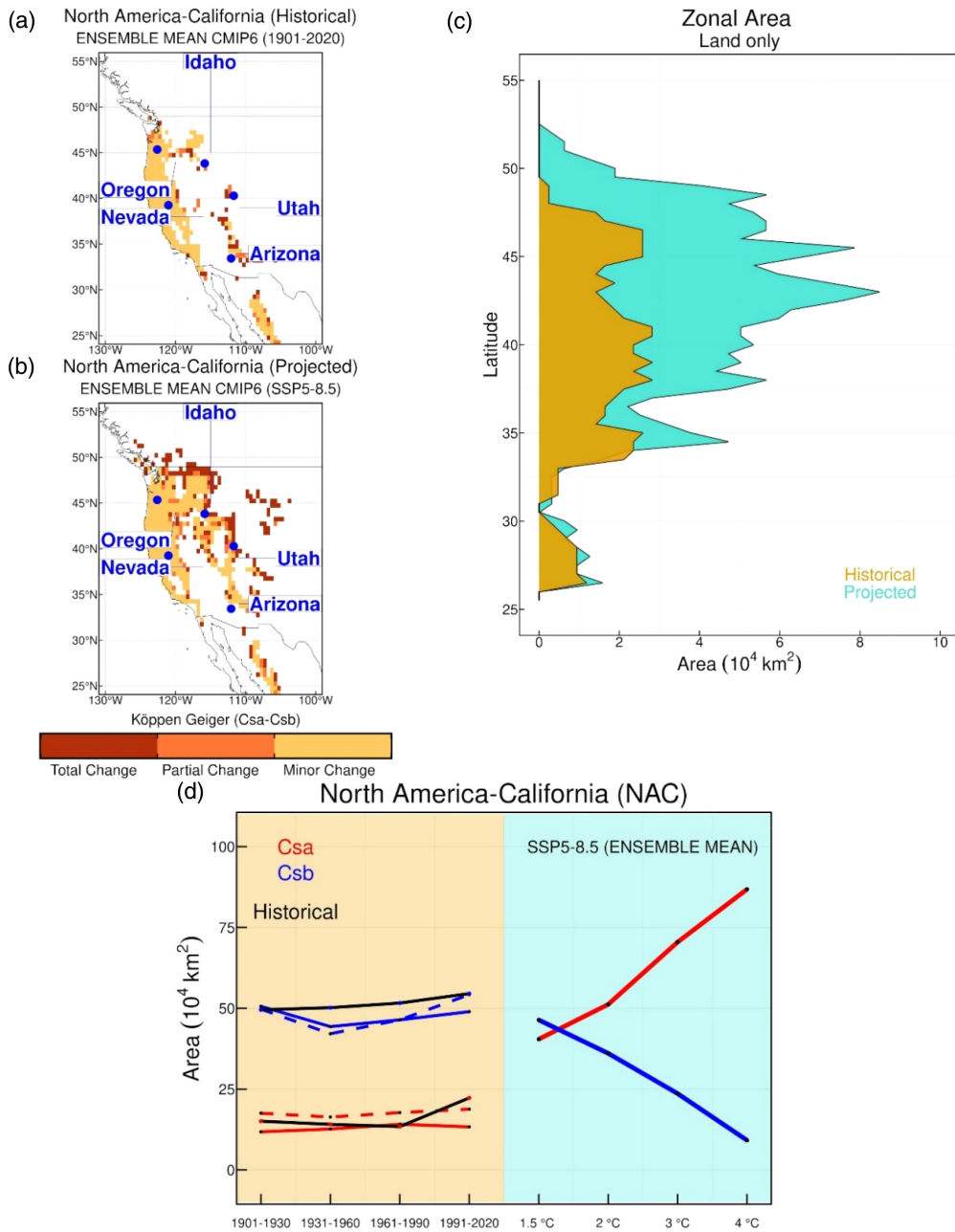


FIGURE 5 | Same as Figure 4, for Mediterranean climate-type regions in North America-California.

(nearly 25%). In SAF, the inter-model agreement is lower, with some models suggesting future increases (e.g., MRI-ESM2-0) and others strong negative signals (e.g., GFDL-ESM4). In all Mediterranean climate-type regions, except for North America-California, the multi-model mean underscores a precipitation decrease with respect to the 1985–2014 reference (Figure 7). Although the regional response to global warming might not be linear, on average, for every additional degree of global warming, the annual precipitation is projected to decrease by about 4%–5% in most of the Mediterranean Basin, Southern Africa, and Southern Australia, while in South America-Central Chile, this decrease is more pronounced (nearly 10%). On the other hand, for every degree of global warming, precipitation will likely increase by about 5% in North America-California.

4 | Discussion

Our analysis assumes that the classes Csa and Csb of the Köppen-Geiger climate classification optimally represent Mediterranean climate-type regions in terms of seasonality, mean and extreme temperatures and precipitation values. Considering the distinct environmental characteristics of MCRs and the fact that this classification system categorises climate zones worldwide based on local vegetation, we consider this hypothesis valid. Furthermore, we assume that concerning the historical and future evolution of MCRs, the bias-corrected and statistically downscaled versions of CMIP6 provide a more detailed and realistic view compared to the original coarse-resolution model output.

TABLE 1 | Percentage of land area for historical conditions and future global warming levels for each class (Arid—B; Temperate other than Csa and Csb—C; Snow—D) according to the Köppen-Geiger climate classification. Regions are defined as (i) Mediterranean Basin—MED (15°W–50°E, 25°–55°N); (ii) North America-California—NAC (125°–110°W, 25°–55°N); (iii) South America-Central Chile—SAC (75°–69°W, 25°–50°S); (iv) Southern Africa—SAF (26°–17°E, 36°–25°S); and (v) Southern Australia—SAU (145°–110°E, 40°–28°S).

MCRs	Category	Historical					Global warming level (°C)				
		1901–1930	1931–1960	1961–1990	1991–2020	1991–2020 minus 1901–1930	1.5	2	3	4	4°C minus 1°C
MED	B	46.7	46.9	47.7	48.1	1.4	48.3	48.5	48.9	49.5	1.2
	C	16.3	15.3	15.0	19.9	3.6	25.1	27.1	32.8	35.9	10.8
	Csa	9.6	9.8	9.2	10.2	0.6	11.0	10.8	10.4	9.8	–1.3
	Csb	3.1	3.1	3.1	2.1	–1.1	1.0	0.6	0.2	0.0	–1.0
	D	24.2	24.9	25.0	19.7	–4.4	14.5	13.0	7.7	4.7	–9.8
NAC	B	43.7	44.5	43.5	42.5	–1.2	42.5	43.7	43.9	44.9	2.3
	C	1.2	1.3	1.6	5.1	4.0	1.8	2.0	5.2	6.9	5.0
	Csa	3.7	3.5	3.3	5.3	1.5	10.0	12.6	17.4	20.8	10.8
	Csb	14.4	14.4	15.1	14.7	0.3	12.9	9.9	6.3	2.3	–10.6
	D	37.1	36.3	36.6	32.4	–4.6	32.7	31.8	27.1	25.2	–7.6
SAC	B	10.2	9.6	16.6	19.9	9.7	15.3	16.3	24.0	20.7	5.5
	C	70.1	70.9	45.7	40.2	–29.9	61.8	61.2	49.6	58.2	–3.6
	Csa	0.0	0.0	0.0	0.5	0.5	0.3	0.8	4.3	6.9	6.6
	Csb	19.7	19.5	37.7	39.3	19.7	22.7	21.6	22.1	14.1	–8.5
	D	0.0	0.0	0.0	0.0	0.0	0.0	0.0	0.0	0.0	0.0
SAF	B	89.0	89.2	89.7	89.7	0.7	92.0	92.3	94.7	93.5	1.5
	C	5.0	4.9	5.7	6.5	1.5	4.2	3.9	2.8	3.6	–0.6
	Csa	2.4	2.4	2.0	1.2	–1.2	2.0	2.5	2.5	3.0	0.9
	Csb	3.5	3.5	2.6	2.6	–0.9	1.8	1.3	0.0	0.0	–1.8
	D	0.0	0.0	0.0	0.0	0.0	0.0	0.0	0.0	0.0	0.0
SAU	B	90.4	90.4	91.2	92.6	2.2	93.1	93.5	93.8	94.5	1.3
	C	1.2	1.5	1.3	1.5	0.2	1.6	1.2	1.3	1.9	0.4
	Csa	2.6	3.2	3.0	2.2	–0.4	2.6	2.4	3.1	3.1	0.5
	Csb	5.7	4.9	4.6	3.7	–2.0	2.7	2.9	1.8	0.5	–2.2
	D	0.0	0.0	0.0	0.0	0.0	0.0	0.0	0.0	0.0	0.0

Note: Bold values represented Mediterranean climate typ-regions (hot-summer--Csa and warm summer--Csb).

For the common MCRs, our findings corroborate previous studies based on different approaches. For example, in the Mediterranean Basin and North America-California, a prominent expansion of temperate regimes by 19% and 23%, respectively, is also evident from the analysis of CMIP5 models and the RCP4.5 pathway for the end of the 21st century (Alessandri et al. 2014). This study also reported a future retreat of temperate zones from lower to higher latitudes (e.g., > 36°N). Moreover, the range of regional temperature and precipitation changes and the comparison with global changes is similar to other studies that used different scenario families or model

ensembles (Cherif et al. 2020; Lionello and Scarascia 2018; Peleg, Bartov, and Morin 2015). The results of this study refer to the high-radiative forcing SSP5-8.5 pathway, quite similar to the RCP8.5 scenarios, at least for the lower GWLs, which were widely used in previous work (Polade et al. 2017). To decrease the uncertainty associated with single-model studies, the results reported in this work are obtained with a bias-corrected and statistically-downscaled ensemble set of projections. These results are slightly different from the spatial expansion of MCRs found by Alessandri et al. (2014) in MED, NAC. For example, they reported a robust expansion

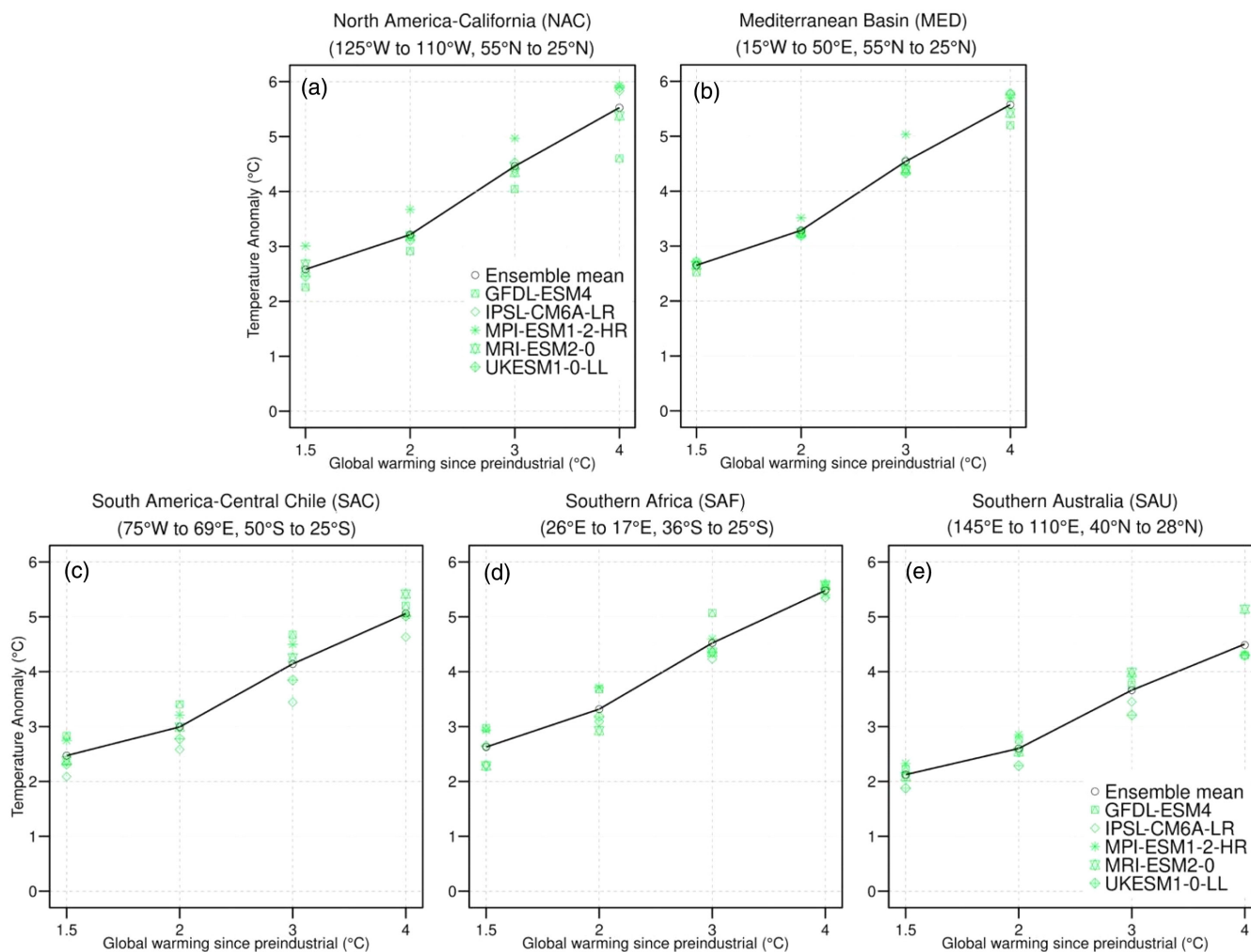


FIGURE 6 | Relationship between global and regional warming levels, with respect to pre-industrial values, based on CMIP6 simulations driven by pathway SSP5-8.5, for five Mediterranean climate-type regions: (a) the Mediterranean Basin (MED), (b) North America-California (NAC), (c) South America-Central Chile (SAC), (d) Southern Africa (SAF), (e) Southern Australia (SAU). Regions are defined as land-only grid-cells.

over the United Kingdom, northern Balkans and Russia. The temperature increase expected by the end of the 21st century for RCP4.5, as analysed by Alessandri et al. (2014), is comparable to the projection for SSP2-4.5 for the same period (Gutiérrez et al. 2021; Iturbide et al. 2021). This similarity also holds for a global warming of 2°C to 3°C under SSP5-8.5 (see Table S2). Therefore, any significant differences in the conclusions between our study and Alessandri et al. (2014) are likely due to variations in the ensemble composition and size, and the use of bias-adjusted model output in our study.

The coarse-resolution output of global climate models (spatial resolution of about 100 km or more) may not be sufficient to account for the complex coastlines and steep elevation gradients often found in MCRs or adjacent climate zones. The coarse resolution smooths relevant temperature and precipitation gradients within the model grid cells, which influences the climate classification results. Therefore, bias-adjusted and downscaled data can provide a more accurate representation of the Köppen-Geiger classification, which relies on absolute thresholds, such as monthly precipitation sums or extreme temperature values. This selection comes at the expense of analysing a smaller size

ensemble, which we believe did not influence our main conclusions. Besides the overall warming and changes in precipitation, future changes in the distribution of global MCRs also rely on changes in the seasonality and extreme values of these parameters, which are critical when applying the Köppen-Geiger classification system. However, a deeper analysis of such changes is beyond the scope of this work and will be better explored in follow-up studies.

5 | Conclusions

Using up-to-date observations and state-of-the-art climate projections, we explored the historical and future changes in the areal extent of Mediterranean climate-type regions globally. These are defined as Csa and Csb zones in the Köppen-Geiger classification. The analysis of historical data highlights that the distribution of MCRs (total Csa and Csb extent) has not changed considerably during the past 120 years. However, future changes will likely occur over a much shorter period (around 40–60 years, according to Table S2). A comparison of historical, observed and future MCRs reveals that the land

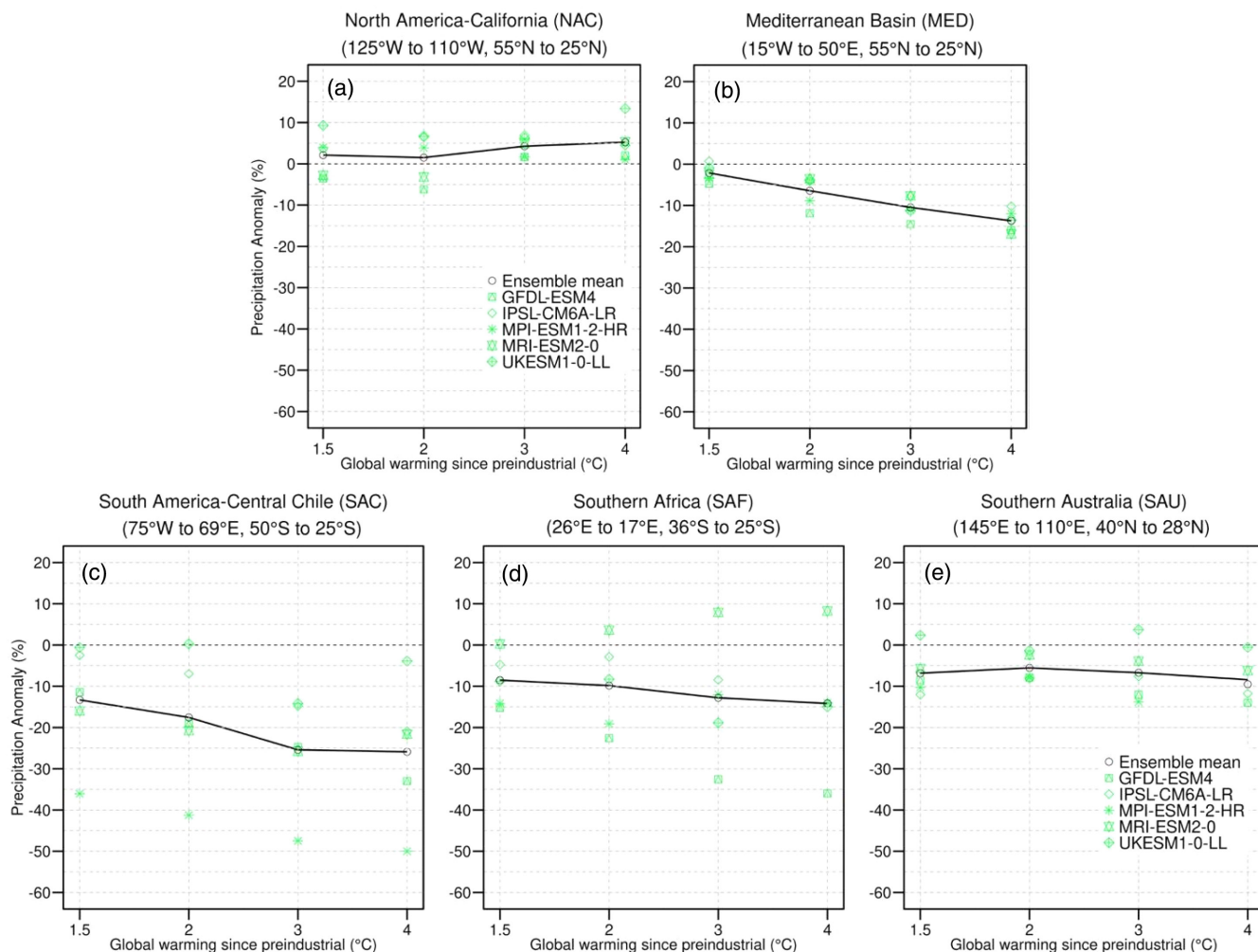


FIGURE 7 | Relationship between global warming levels (since pre-industrial) and precipitation, with respect to the 1985–2014 reference period, based on CMIP6 global simulations driven by pathway SSP5-8.5, for five Mediterranean climate-type regions: (a) the Mediterranean Basin (MED), (b) North America-California (NAC), (c) South America-Central Chile (SAC), (d) Southern Africa (SAF), (e) Southern Australia (SAU). Regions are defined as land-only grid-cells.

areas involved will change dramatically, implying MCRs will expand by around 5.8% or $18 \times 10^4 \text{ km}^2$. In the Mediterranean Basin, North America-California and South America-Central Chile, this will occur as a poleward and eastward expansion of MCRs. In Southern Africa and Southern Australia, MCRs are expected to diminish, particularly for high global warming levels. The future decline of precipitation, except for North America-California, and the more pronounced temperature increase will imply total and partial changes in climate regimes over most MCRs (about 75% of their area). The most widespread future changes will be from temperate to hot-arid zones. At the same time, large regions characterised as warm-summer Mediterranean-type zones (Csb) will likely transition to hot-summer climate zones (Csa), a pattern that is already evident in the historical period.

According to the CMIP6 projections, future regional warming in the broader MCR zones is robust (strong inter-model agreement) and stronger than the mean global warming levels. This is primarily the case for the Northern Hemisphere MCRs in the Mediterranean and California regions.

Regarding precipitation changes, for every additional degree of global warming, precipitation is projected to decrease by about 5%–10% in the Mediterranean Basin, Southern Africa, Southern Australia and South America-Central Chile. On the other hand, for every degree of global warming, mean rainfall will increase by about 5% in the North America-California region, but this change is mostly not statistically significant (Gutiérrez et al. 2021).

Author Contributions

Diego Urdiales-Flores: conceptualization, investigation, methodology, validation, visualization, writing – review and editing, writing – original draft, formal analysis, data curation. **George Zittis:** conceptualization, investigation, funding acquisition, methodology, validation, visualization, writing – review and editing, formal analysis, project administration, data curation, supervision, resources, writing – original draft. **Panos Hadjinicolaou:** conceptualization, investigation, funding acquisition, methodology, validation, visualization, writing – review and editing, formal analysis, project administration, data curation, supervision, resources. **Annalisa Cherchi:** writing – review and editing, methodology, formal analysis, investigation, conceptualization.

Andrea Alessandri: conceptualization, investigation, methodology, formal analysis, writing – review and editing. **Nadav Peleg:** conceptualization, investigation, writing – review and editing. **Jos Lelieveld:** conceptualization, writing – review and editing, project administration, supervision, resources.

Acknowledgements

We acknowledge the World Climate Research Programme's Working Group on Coupled Modelling, which is responsible for CMIP, and we thank the climate modelling groups for producing and making available their model output. This research was supported by the EMME-CARE project that has received funding from the European Union's Horizon 2020 Research and Innovation Program, under Grant Agreement No., 856612, as well as matching co-funding by the Government of Cyprus. D.U.F. was supported by the Swiss Government Excellence Scholarships 2023/2024 which has received funding from the Swiss State Secretariat for Education and Innovation. G.Z., A.C. and A.A. were funded by the European Union's Horizon Europe Research and Innovation Program under Grant Agreement no. 101081193 (OptimESM project). A.C. and A.A. acknowledge support from ICSC—Centro Nazionale di Ricerca in High Performance Computing, Big Data and Quantum Computing, funded by European Union—NextGenerationEU (Concession Decree N. 1031 of 17/06/2022 adopted by the Italian Ministry of University and Research). N.P. was supported by the Swiss National Science Foundation (SNSF), Grant 194649 ('Rainfall and floods in future cities'). The authors wish to thank Dr. Jose Araya for providing CMIP6 datasets and Mr. Gabriel Gaona for support during the analysis.

Ethics Statement

The authors have nothing to report.

Conflicts of Interest

The authors declare no conflicts of interest.

Data Availability Statement

All data used in the present analysis are open-access. Sources are presented in the Methods Section. The R package "ClimClass" (Eccel et al. 2016) was used to perform the global Köppen-Geiger climate classification. The R package "ClimProjDiags" (Perez-Zanon and Hunter 2024) was used for spatial area-weighted average anomalies analysis.

Endnotes

¹ https://www.isimip.org/documents/356/ISIMIP-FT_Protocol_16Oct2018.pdf.

² https://github.com/IPCC-WG1/Atlas/blob/main/warming-levels/CMIP6_Atlas_WarmingLevels.csv.

References

- Alessandri, A., M. De Felice, N. Zeng, et al. 2014. "Robust Assessment of the Expansion and Retreat of Mediterranean Climate in the 21st Century." *Scientific Reports* 4: 4–11. <https://doi.org/10.1038/srep07211>.
- Ali, E., W. Cramer, J. Carnicer, et al. 2022. "Cross-Chapter Paper 4: Mediterranean Region." In *Climate Change 2022: Impacts, Adaptation and Vulnerability. Contribution of Working Group II to the Sixth Assessment Report of the Intergovernmental Panel on Climate Change*, edited by H.-O. Pörtner, D. C. Roberts, M. Tignor, E. S. Poloczanska, K. Mintenbeck, A. Alegria, M. Craig, S. Langsdorf, S. Löschke, V. Möller, A. Okem, and B. Rama, 2233–2272. Cambridge, UK and New York, NY, USA: Cambridge University Press. <https://doi.org/10.1017/9781009325844.021>.
- Allen, R. J., and O. Ajoku. 2016. "Future Aerosol Reductions and Widening of the Northern Tropical Belt." *Journal of Geophysical Research* 121, no. 12: 6765–6786. <https://doi.org/10.1002/2016JD024803>.

- Amaya, D. J., N. Siler, S. P. Xie, and A. J. Miller. 2018. "The Interplay of Internal and Forced Modes of Hadley Cell Expansion: Lessons From the Global Warming Hiatus." *Climate Dynamics* 51, no. 1–2: 305–319. <https://doi.org/10.1007/s00382-017-3921-5>.
- Araya-Osses, D., A. Casanueva, C. Román-Figueroa, J. M. Uribe, and M. Paneque. 2020. "Climate Change Projections of Temperature and Precipitation in Chile Based on Statistical Downscaling." *Climate Dynamics* 54: 4309–4330. <https://doi.org/10.1007/s00382-020-05231-4>.
- Barcikowska, M. J., S. B. Kapnick, L. Krishnamurty, S. Russo, A. Cherchi, and C. K. Folland. 2020. "Changes in the Future Summer Mediterranean Climate: Contribution of Teleconnections and Local Factors." *Earth System Dynamics* 11, no. 1: 161–181.
- Beck, H. E., N. E. Zimmermann, T. R. McVicar, N. Vergopolan, A. Berg, and E. F. Wood. 2018. "Present and Future Köppen-Geiger Climate Classification Maps at 1-km Resolution." *Scientific Data* 5: 1–12. <https://doi.org/10.1038/sdata.2018.214>.
- Behnke, R., S. Vavrus, A. Allstadt, T. Albricht, W. E. Thogmartin, and V. C. Radeloff. 2016. "Evaluation of Downscaled, Gridded Climate Data for the Conterminous United States." *Ecological Applications* 26, no. 5: 1338–1351.
- Cai, W., A. Santoso, G. Wang, et al. 2015. "ENSO and Greenhouse Warming." *Nature Climate Change* 5, no. 9: 849–859. <https://doi.org/10.1038/nclimate2743>.
- Campins, J., A. Genovés, M. A. Picornell, and A. Jansà. 2011. "Climatology of Mediterranean Cyclones Using the ERA-40 Dataset." *International Journal of Climatology* 31, no. 11: 1596–1614. <https://doi.org/10.1002/joc.2183>.
- Cheng, W., L. Dan, X. Deng, et al. 2022. "Global Monthly Gridded Atmospheric Carbon Dioxide Concentrations Under the Historical and Future Scenarios." *Scientific Data* 9, no. 1: 83. <https://doi.org/10.1038/s41597-022-01196-7>.
- Cherchi, A., T. Ambrizzi, B. Swadhin, V. F. A. Carolina, M. Yushi, and Z. Tianjun. 2018. "The Response of Subtropical Highs to Climate Change." *Current Climate Change Reports* 4: 371–382.
- Cherif, S., E. Doblas-Miranda, P. Lionello, et al. 2020. "Chapter 2 Drivers of Change." In *Climate and Environmental Change in the Mediterranean Basin – Current Situation and Risks for the Future. First Mediterranean Assessment Report*, edited by W. Cramer, J. Guiot, and K. Marini, 59–180. Marseille, France: Union for the Mediterranean, Plan Bleu, UNEP/MAP.
- Chua, Z. W., Y. Kuleshov, A. B. Watkins, S. Choy, and C. Sun. 2022. "A Two-Step Approach to Blending GSMaP Satellite Rainfall Estimates With Gauge Observations Over Australia." *Remote Sensing* 14, no. 8: 1903.
- Deitch, M., M. Sapundjieff, and S. Feirer. 2017. "Characterizing Precipitation Variability and Trends in the World's Mediterranean-Climate Areas." *Water* 9, no. 4: 259. <https://doi.org/10.3390/w9040259>.
- Dey, R., S. C. Lewis, J. M. Arblaster, and N. J. Abram. 2019. "A Review of Past and Projected Changes in Australia's Rainfall." *Wiley Interdisciplinary Reviews: Climate Change* 2019, no. 10: e577.
- Douville, H., K. Raghavan, J. Renwick, et al. 2021. "Water Cycle Changes." In *Climate Change 2021: The Physical Science Basis. Contribution of Working Group I to the Sixth Assessment Report of the Intergovernmental Panel on Climate Change*, edited by V. Masson-Delmotte, P. Zhai, A. Pirani, S. L. Connors, C. Péan, S. Berger, N. Caud, Y. Chen, L. Goldfarb, M. I. Gomis, M. Huang, K. Leitzell, E. Lonnoy, J. B. R. Matthews, T. K. Maycock, T. Waterfield, O. Yelekçi, R. Yu, and B. Zhou, 1055–1210. Cambridge, United Kingdom and New York, NY, USA: Cambridge University Press. <https://doi.org/10.1017/9781009157896.010>.
- Eccel, E., E. Cordanò, and G. Toller. 2016. "ClimClass: Climate Classification According to Several Indices." R package version 2.1.0. <https://CRAN.R-project.org/package=ClimClass>.

- Faticchi, S., N. Peleg, T. Mastrotheodoros, C. Pappas, and G. Manoli. 2021. "An Ecohydrological Journey of 4500 Years Reveals a Stable but Threatened Precipitation–Groundwater Recharge Relation Around Jerusalem." *Science Advances* 7, no. 37: eabe6303.
- Flocas, H. A., I. Simmonds, J. Kouroutzoglou, et al. 2010. "On Cyclonic Tracks Over the Eastern Mediterranean." *Journal of Climate* 23, no. 19: 5243–5257. <https://doi.org/10.1175/2010JCLI3426.1>.
- Gutiérrez, J. M., R. G. Jones, G. T. Narisma, et al. 2021. "Atlas." In *Climate Change 2021: The Physical Science Basis. Contribution of Working Group I to the Sixth Assessment Report of the Intergovernmental Panel on Climate Change*, edited by V. Masson-Delmotte, P. Zhai, A. Pirani, S. L. Connors, C. Péan, S. Berger, N. Caud, Y. Chen, L. Goldfarb, M. I. Gomis, M. Huang, K. Leitzell, E. Lonnoy, J. B. R. Matthews, T. K. Maycock, T. Waterfield, O. Yelekçi, R. Yu, and B. Zhou, 1927–2058. Cambridge, United Kingdom and New York, NY: Cambridge University Press. Interactive Atlas. <https://doi.org/10.1017/9781009157896.021>.
- Hagemann, S., C. Chen, J. O. Haerter, J. Heinke, D. Gerten, and C. Piani. 2011. "Impact of a Statistical Bias Correction on the Projected Hydrological Changes Obtained From Three GCMs and Two Hydrology Models." *Journal of Hydrometeorology* 12, no. 4: 556–578.
- Hannah, L., P. R. Roehrdanz, M. Ikegami, et al. 2013. "Climate Change, Wine, and Conservation." *Proceedings of the National Academy of Sciences* 110, no. 17: 6907–6912.
- Harris, I., T. J. Osborn, P. Jones, and D. Lister. 2020. "Version 4 of the CRU TS Monthly High-Resolution Gridded Multivariate Climate Dataset." *Scientific Data* 7, no. 1: 1–18. <https://doi.org/10.1038/s41597-020-0453-3>.
- IPCC. 2021. "Climate Change 2021. The Physical Science Basis. Contribution of Working Group 1 to Sixth Assessment Report of the Intergovernmental Panel on Climate Change." <https://www.ipcc.ch/report/ar6/wg1/>.
- Iturbide, M., J. Fernández, J. M. Gutiérrez, et al. 2021. "Repository Supporting the Implementation of FAIR Principles in the IPCC-WG1 Atlas." Zenodo. <https://doi.org/10.5281/zenodo.3691645> <https://github.com/IPCC-WG1/Atlas>.
- Kang, S. M., L. M. Polvani, J. C. Fyfe, and M. Sigmond. 2011. "Impact of Polar Ozone Depletion on Subtropical Precipitation." *Science* 332, no. 6032: 951–954.
- Köppen, W. 1900. "Versuch einer Klassifikation der Klimate, vorzugsweise nach ihren Beziehungen zur Pflanzenwelt.(Schluss)." *Geographische Zeitschrift* 6, no. 12. H: 657–679.
- Kottek, M., J. Grieser, C. Beck, B. Rudolf, and F. Rubel. 2006. "World Map of the Köppen-Geiger Climate Classification Updated." *Meteorologische Zeitschrift* 15, no. 3: 259–263. <https://doi.org/10.1127/0941-2948/2006/0130>.
- Kovilakam, M., and S. Mahajan. 2015. "Black Carbon Aerosol-Induced Northern Hemisphere Tropical Expansion." *Geophysical Research Letters* 42, no. 12: 4964–4972. <https://doi.org/10.1002/2015GL064559>.
- Lange, S., and M. Büchner. 2020. "ISIMIP2a Atmospheric Climate Input Data." ISIMIP Repository. <https://doi.org/10.48364/ISIMIP.886955>.
- Lange, S., and M. Büchner. 2021. "ISIMIP3b bias-adjusted atmospheric climate input data (v1. 1)."
- Lazenby, M. J., M. C. Todd, R. Chadwick, and Y. Wang. 2018. "Future Precipitation Projections Over Central and Southern Africa and the Adjacent Indian Ocean: What Causes the Changes and the Uncertainty?" *Journal of Climate* 31, no. 12: 4807–4826.
- Lionello, P. 2012. *The Climate of the Mediterranean Region: From the Past to the Future* (1st ed.). Elsevier, London and Waltham, MA: Elsevier Insights.
- Lionello, P., and L. Scarascia. 2018. "The Relation Between Climate Change in the Mediterranean Region and Global Warming." *Regional Environmental Change* 18, no. 5: 1481–1493. <https://doi.org/10.1007/s10113-018-1290-1>.
- Liu, W., F. Sun, Y. Feng, et al. 2021. "Increasing Population Exposure to Global Warm-Season Concurrent Dry and Hot Extremes Under Different Warming Levels." *Environmental Research Letters* 16, no. 9: 0904002. <https://doi.org/10.1088/1748-9326/ac188f>.
- Mantsis, D. F., S. Sherwood, R. Allen, and L. Shi. 2017. "Natural Variations of Tropical Width and Recent Trends." *Geophysical Research Letters* 44, no. 8: 3825–3832. <https://doi.org/10.1002/2016GL072097>.
- Mariotti, A., and A. Dell'Aquila. 2012. "Decadal Climate Variability in the Mediterranean Region: Roles of Large-Scale Forcings and Regional Processes." *Climate Dynamics* 38: 1129–1145.
- Min, S. K., and S. W. Son. 2013. "Multimodel Attribution of the Southern Hemisphere Hadley Cell Widening: Major Role of Ozone Depletion." *Journal of Geophysical Research-Atmospheres* 118, no. 7: 3007–3015. <https://doi.org/10.1002/jgrd.50232>.
- Morin, E. 2011. "To Know What We Cannot Know: Global Mapping of Minimal Detectable Absolute Trends in Annual Precipitation." *Water Resources Research* 47, no. 7. <https://doi.org/10.1029/2010WR009798>.
- Myers, N., R. A. Mittermeier, C. G. Mittermeier, G. A. B. Fonseca, and J. Kent. 2000. "Biodiversity Hotspots for Conservation Priorities." *Nature* 403, no. 6772: 853–858.
- Nikulin, G., C. Lennard, A. Dosio, et al. 2018. "The Effects of 1.5 and 2 Degrees of Global Warming on Africa in the CORDEX Ensemble." *Environmental Research Letters* 13, no. 6: 065003. <https://doi.org/10.1088/1748-9326/aab1b1>.
- Perez-Zanon, N., and A. Hunter. 2024. "ClimProjDiags: Set of Tools to Compute Various Climate Indices." R package version 0.3.3. <https://CRAN.R-project.org/package=ClimProjDiags>.
- Peleg, N., M. Bartov, and E. Morin. 2015. "CMIP5-Predicted Climate Shifts Over the East Mediterranean: Implications for the Transition Region Between Mediterranean and Semi-Arid Climates." *International Journal of Climatology* 35, no. 8: 2144–2153. <https://doi.org/10.1002/joc.4114>.
- Petrie, R., S. Denvil, S. Ames, et al. 2021. "Coordinating an Operational Data Distribution Network for CMIP6 Data." *Geoscientific Model Development* 14, no. 1: 629–644. <https://doi.org/10.5194/gmd-14-629-2021>.
- Piani, C., G. P. Weedon, M. Best, et al. 2010. "Statistical Bias Correction of Global Simulated Daily Precipitation and Temperature for the Application of Hydrological Models." *Journal of Hydrology* 395, no. 3–4: 199–215.
- Polade, S. D., A. Gershunov, D. R. Cayan, M. D. Dettinger, and D. W. Pierce. 2017. "Precipitation in a Warming World: Assessing Projected Hydro-Climate Changes in California and Other Mediterranean Climate Regions." *Scientific Reports* 7, no. 1: 1–10. <https://doi.org/10.1038/s41598-017-11285-y>.
- Rodwell, M. J., and B. J. Hoskins. 2001. "Subtropical Anticyclones and Summer Monsoons." *Journal of Climate* 14, no. 15: 3192–3211. [https://doi.org/10.1175/1520-0442\(2001\)014<3192:SAASM>2.0.CO;2](https://doi.org/10.1175/1520-0442(2001)014<3192:SAASM>2.0.CO;2).
- Seager, R., R. Murtugudde, N. Naik, A. Clement, N. Gordon, and J. Miller. 2003. "Air-Sea Interaction and the Seasonal Cycle of the Subtropical Anticyclones." *Journal of Climate* 16, no. 12: 1948–1966. [https://doi.org/10.1175/1520-0442\(2003\)016<1948:AIATSC>2.0.CO;2](https://doi.org/10.1175/1520-0442(2003)016<1948:AIATSC>2.0.CO;2).
- Seager, R., T. J. Osborn, Y. Kushnir, I. R. Simpson, J. Nakamura, and H. Liu. 2019. "Climate Variability and Change of Mediterranean-Type Climates." *Journal of Climate* 32, no. 10: 2887–2915. <https://doi.org/10.1175/JCLI-D-18-0472.1>.
- Sylla, M. B., F. Giorgi, E. Coppola, and L. Mariotti. 2013. "Uncertainties in Daily Rainfall Over Africa: Assessment of Gridded Observation

Products and Evaluation of a Regional Climate Model Simulation.” *International Journal of Climatology* 33: 1805–1817.

Taschetto, A. S., C. C. Ummenhofer, M. F. Stuecker, et al. 2020. “ENSO Atmospheric Teleconnections.” In *El Niño Southern Oscillation in a Changing Climate*, 309–335. Washington, DC: American Geophysical Union. <https://doi.org/10.1002/9781119548164.ch14>.

Tebaldi, C., K. Debeire, V. Eyring, et al. 2021. “Climate Model Projections From the Scenario Model Intercomparison Project (ScenarioMIP) of CMIP6.” *Earth System Dynamics* 12, no. 1: 253–293. <https://doi.org/10.5194/esd-12-253-2021>.

Urdiales, D., F. Meza, J. Gironás, and H. Gilabert. 2018. “Improving Stochastic Modelling of Daily Rainfall Using the ENSO Index: Model Development and Application in Chile.” *Water* 10, no. 2: 145. <https://doi.org/10.3390/w10020145>.

Urdiales-Flores, D., G. Zittis, P. Hadjinicolaou, et al. 2023. “Drivers of Accelerated Warming in Mediterranean Climate-Type Regions.” *npj Climate and Atmospheric Science* 6, no. 1. <https://doi.org/10.1038/s41612-023-00423-1>.

Vogiatzakis, I. N., A. M. Mannion, and D. Sarris. 2016. “Mediterranean Island Biodiversity and Climate Change: The Last 10,000 Years and the Future.” *Biodiversity and Conservation* 25, no. 13: 2597–2627. <https://doi.org/10.1007/s10531-016-1204-9>.

Zelinka, M. D., T. A. Myers, D. T. McCoy, et al. 2020. “Causes of Higher Climate Sensitivity in CMIP6 Models.” *Geophysical Research Letters* 47, no. 1: e2019GL085782.

Zittis, G. 2018. “Observed Rainfall Trends and Precipitation Uncertainty in the Nivity of the Mediterranean, Middle East and North Africa.” *Theoretical and Applied Climatology* 134, no. 3–4: 1207–1230.

Zittis, G., M. Almazroui, P. Alpert, et al. 2022. “Climate Change and Weather Extremes in the Eastern Mediterranean and Middle East.” *Reviews of Geophysics* 60, no. 3. <https://doi.org/10.1029/2021RG000762>.

Zittis, G., P. Hadjinicolaou, M. Klangidou, Y. Proestos, and J. Lelieveld. 2019. “A Multi-Model, Multi-Domain and Multi-Scenario Analysis of Regional Climate Projections for the Mediterranean.” *Regional Environmental Change* 19, no. 8: 2621–2635. <https://doi.org/10.1007/s10113-019-01565-w>.

Zittis, G., A. Bruggeman, and J. Lelieveld. 2021. “Revisiting Future Extreme Precipitation Trends in the Mediterranean.” *Weather and Climate Extremes* 34, no. August: 100380. <https://doi.org/10.1016/j.wace.2021.100380>.

Supporting Information

Additional supporting information can be found online in the Supporting Information section.